GEOPHYSICS, VOL. 66, NO. 5 (SEPTEMBER-OCTOBER 2001); P. 1569–1581, 12 FIGS., 2 TABLES.

Numerical modeling and interpretation of drillstring waves

Flavio Poletto≫, Massimo Malusa≫, and Francesco Miranda‡

ABSTRACT

Drill-bit seismic and pilot seismograms contain drillstring periodicities from signal and environmental noise sources. These coherent components are similar in seismic-while-drilling correlations, and their joint contribution may cause distortions in signal processing. Numeric modeling of the drillstring transmission line is used to correctly interpret the axial and torsional events with similar propagating modes of signal and noise. The reflection coefficients are computed for drillstrings of arbitrary materials, and their average mechanical features are related to the axial and torsional group velocities obtained by the dispersion equations. Fitting of the periodical components in the real seismograms is used to automatically correct the drill-bit pilot delays and to estimate the surface and downhole boundary conditions.

INTRODUCTION

The vibrations of a working drill bit are measured in two different ways for seismic-while-drilling surveying. The reference pilot signal is obtained by measuring the energy transmitted through the drillstring. It is usually recorded by surface sensors placed on the drilling rig (Rector and Marion, 1991). In particular applications, the pilot signal can also be measured near the bit. A second type of signal is recorded by seismic lines placed at the surface or in neighboring wells. This is the seismic signal transmitted through the formations. These two signals are crosscorrelated to get a real-time reverse vertical seismic profile (VSP) (Figure 1). This process attenuates the random noise caused by the drilling yard activity and simultaneously reinforces the in-phase signal. However, it also reinforces the coherent contribution of undesired environmental noise and drillstring vibrations. These vibrations are well known to drillers, who avoid particular drilling parameters which cause resonance and affect drilling efficiency. Yet a remarkable number of these vibrations are generated during normal drilling conditions. For this reason, the autocorrelation of the rig pilot signal and the crosscorrelations of the rig pilot signal with the seismic field data each have a distinct drillstring response. These correspond to various propagating modes. To improve the pilot signal and remove its propagation effects, two other processing steps can be applied after correlation: the pilot signal deconvolution and the correction of the absolute seismic time (Rector and Marion, 1991), which is calibrated by analyzing the reflectivity in the drillstring. The deconvolution is applied to remove the reflections and the periodic events of the signal transmitted through the drillstring. The time correction is applied to remove the delay of the signal transmitted in the drillstring from the bit source to the pilot receiver. This correction is deterministic if the propagation velocity in the drillstring is known.

The complex dynamic behavior of the drillstring has been the object of investigation since the early 1960s. Studies on the behavior of the drillstring and rig structure system tried to achieve a theoretical model to support the drillers and supply information about the bit and drillstring's state of wear. Lutz et al. (1972) developed a theoretical interpretation of axial vibrations transmitted to the rock and the drill system by a rotating tricone bit to obtain information on rock properties.

More recently, the acoustic vibrations of the drillstring were investigated to evaluate the potential of elastic waves for transmitting information between the drill bit and the rig operator during drilling operations (Drumheller, 1989, 1992, 1993). Drumheller's analysis considered frequencies of up to 2000 Hz. He found that the propagating energy is attenuated according to the frequency and the coupling between the drillstring and mud. Not considering the effects of the rock around the drillstring, he showed that the periodically spaced discontinuities of tool joints cause stop bands and pass bands for acoustic transmission through drillpipes (Barnes and Kirkwood, 1972), and change the group velocity (Drumheller and Knudsen, 1995). A detailed discussion about acoustic properties of the drillstring is given by Carcione and Poletto (2000). They solve the differential equations by a pseudospectral method to model the geometric features of pipes and coupling joints. Their equations include relaxation mechanisms simulating the viscoelastic behavior of the steel and any losses, such as those

Manuscript received by the Editor September 7, 1999; revised manuscript received November 2, 2000.
≫Istituto Nazionale di Oceanografia e di Geofisica Sperimentale—OGS, Borgo Grotta Gigante no. 42/c, 34010 Sgonico, Trieste, Italy. E-mail: fpoletto@ogs.trieste.it; mmalusa@ogs.trieste.it.
‡Eni S.p.A.—Divisione Agip, via Europa Unita 3, 20097 S. Donato Milanese, Milano, Italy. E-mail: francesco.miranda@agip.it.

produced by the presence of the drilling mud, the casing, and the formation.

In this decade, the working drill bit was used as a seismic source for reverse (VSP) and to monitor the evolution of the well (Haldorsen et al., 1995; Miranda et al., 1996; Angeleri et al., 1990; Rocca et al., 1990). However, by acquiring data with surface measurements only, this technique is restricted to low-frequency bands (<120 Hz). It mainly observes long-period reverberations and bottom-hole-assembly (BHA) multiples.

Rector (1989) introduced a reference deconvolution method in which the signal detected at the top of the drillstring was used to develop an operator to reduce the amplitude of the drillstring multiples in the field seismic traces. A critical point in this approach is that it is completely data dependent and therefore is influenced by dynamic boundary conditions, bit-rock coupling, and surface noise. Using rig measurements, Booer and Meehan (1993) developed a model-based approach to analyze the drillstring vibrations; the resulting image allowed identified the reflection coefficient at the bit and at the intermediate points in the drillstring. They used an inverse approach to get reflection coefficients from rig surface measurements of hook load and torque.

In this paper, we interpret the vibrations measured by the Seisbit seismic-while-drilling system (Miranda et al., 1996) using drillstring waves propagating in the drillstring and in the formations (Malusa et al., 1997). We consider the periodic coherent events generated by the downhole signal and the surface rig noise. Our proposed model characterizes the waves propagating through the drill pipes and the dynamic behavior of the system comprised of by the derrick, drillstring, and rocks.

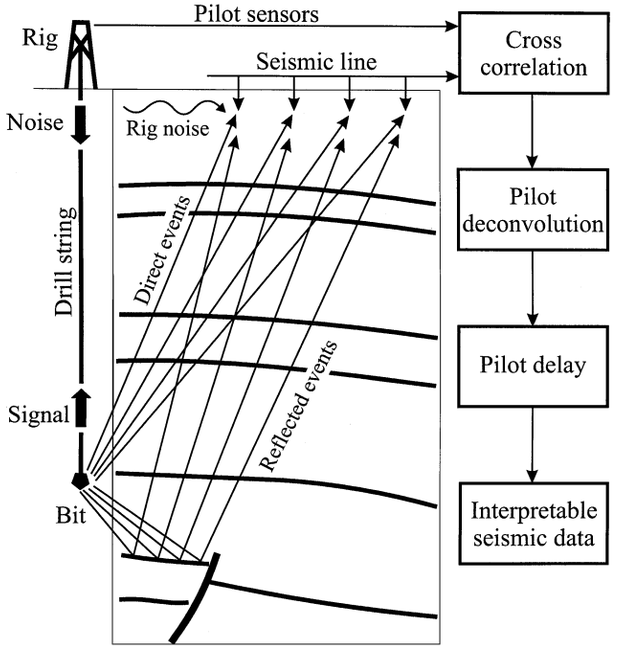

FIG. 1. The seismic-while-drilling technique utilizes the vibration produced by a working drill bit as a downhole seismic source. The drill-bit signal propagates through the drillstring to the pilot sensors placed on the rig. At the other end, the signal propagates through the formations and is recorded by the seismic line placed on the ground. The crosscorrelation of these two signals is used to get a reverse VSP.

Assuming, without loss of generality, that the drill-bit signals and noise sources are white, we parameterize a 1-D transmission-line model using the drilling information, such as the string length and kelly position, and consider the mechanical features of the drillstring to get its reflection coefficients. We do not consider the interaction of the drillstring with the casing and the formations at intermediate contact points.

Synthetic seismograms are automatically obtained while drilling by changing trial boundary conditions to fit the data. This simple approach allows us to validate the wavefield interpretation, locating the bit on the pilot seismograms. At the same time, it provides the means for detecting the downhole drilling conditions that influence the bit signal. It also gives information about the radiated signal and the coherent noise, which have, in the correlated pilot and seismic data, similar trends of periodicity. In particular, the long-period drillstring signal multiples can be confused with the correlated surface rig noise.

In this paper we first describe the types of vibrations propagating in the drillstring from the working drill bit and surface rig noise and their dependence on drillstring features. Second, we analyze the contribution of drillstring events to the correlated seismograms. Then we describe the transmission-line modeling of the drillstring on the basis of the axial and torsional reflection coefficients and the fitting procedure. Finally, we interpret the signal and noise contributions and discuss the results.

DRILLSTRING VIBRATIONS

Knowledge of mechanical features of the drillstring is necessary to correctly recognize periodic reverberations. The drillstring can be divided into two main parts (Figure 2). The upper part is the drill pipe, composed of a sequence of nonhomogeneous elements with more or less the same dimension and weight. Each length of pipe is composed of a body and is connected to the other pipe lenths by tool joints that are thicker and heavier than the body. The drillstring can have different sections of pipe with different tool joints. Table 1 shows a typical classification for the drill-pipe components according to yield strength. In our experience, the types of drill pipe used most often are S,G, and E. Another important parameter is the class of wear state. Drill pipe is subclassified as new, premium (corresponding to $< 20\%$ wear), class 2, and class 3.

The lower part of the drillstring is the bottom-hole assembly (BHA). This section is more massive and its composition is rather complex. It is made up of various components of different dimensions and mechanical characteristics. The most important are the heavyweight drill pipe and drill collars. These BHA components cause important variations of impedance and strong reverberations in the pilot and seismic data.

The type of drill bit has a major influence on the vibrations induced in the drillstring. Generally, a good signal is generated by a roller-cone bit, which provides strong axial vibrations in the

Table 1. Classification of drill-pipe components

Type of drill pipe	Yield strength (psi)
D	55 000 ≫ 85 000
E	75 000 ≫ 105 000
X	95 000 ≫ 125 000
G	105 000 ≫ 135 000
S	135 000 ≫ 165 000

drillstring and in the ground (Rector and Hardage, 1992). On the other hand, a polycrystalline diamond compacts (PDC) bit, acting mainly as a shearing tool, produces lower axial signals (Poletto et al., 1997). Another important characteristic of the bit is its state of wear. A new roller-cone bit produces more vibrations than a dull bit. Colored components, such as the roller-cone trilobe pattern, are generated by the working bits and can be influenced by several downhole dynamic drilling phenomena, such as bouncing and whirling (Hutchinson et al., 1995). The signal features are also linked to the type of drilled rock and drilling conditions, since higher pilot amplitude vibrations are observed in harder rocks. However, the method provides usable data in various types of lithology. Operational conditions, such as the frequency of rotation and the weight on bit, influence the bit–rock coupling, the amount of emitted energy, and the quality of the pilot signal. For a constant introduced energy, the amplitude of the vibrations recorded by the pilot sensors decreases when the rate of penetration increases (Raynal et al., 1973).

COMPONENT	PARTIAL LENGTH (m)	CUMULATIVE LENGTH(m)	O.D. (inch)	I.D. (inch)	PARTIAL WEIGHT IN AIR (t)	PARTIAL WEIGHT IN MUD (t)
DP 5" S135	5258,84	5258,84	5"	4"9/32	173,542	150,139
N° 15 HWDP	137,99	5396,83	5"	3"	183,753	158,974
XO	0,47	5397,3	6"1/2	2"13/16	183,788	159,004
N° 3 DC	27,58	5424,88	6"1/2	2"7/8	187,6	162,3
JAR	10,33	5435,21	6"1/4	2"1/2	189,0	163,5
N° 8 DC	75,40	5510,61	6"1/2	2"7/8	199,3	172,4
STAB	1,89	5512,50	6"1/4	2"13/16	199,6	172,7
N° 2 DC (slc)	18,65	5531,15	6"1/2	2"7/8	202,1	174,9
N° 2 DC	18,65	5549,80	6"1/2	2"7/8	204,7	177,1
STAB	1,48	5532,63	6"3/4	2"13/16	202,3	175,0
KEY SIT WIPER	1,48	5551,28	6"3/4	2"13/16	204,9	177,3
N° 1 DC (slc)	9,46	5542,09	6"1/2	2"7/8	203,6	176,2
N° 1 DC (sp)	9,46	5551,55	6"1/2	2"7/8	204,9	177,3
MONEL	9,46	5551,55	6"1/2	2"7/8	204,9	177,3
MWD	9,46	5561,01	6"1/2	2"7/8	206,2	178,4
XO	0,66	5542,75	6"1/4	2"13/16	203,7	176,2
BIT	0,25	5543,00	8"1/2		203,7	176,3

FIG. 2. Sample of a table showing the drillstring mechanical properties. This table is available at the rig site and can be used easily to compute the numerical model of the drillstring. The first, higher row describes the drill-pipe section. The other rows describe the BHA components, with different dimensions and mechanical characteristics.

A working drill bit induces axial, torsional, and flexural vibrations in the drillstring, which can propagate with a wide frequency band—from 1 Hz to 2 KHz (Drumheller, 1989). The flexural waves, owing to the presence of the mud in the borehole, are dispersive and cannot be used easily as a communication tool between the lower and upper hole. On the contrary, at low frequencies the wavelength of the extensional–axial and torsional–transverse components are long compared to the drillstring diameter, so they are not dispersive. These axial and torsional vibrations are recorded by the pilot sensors placed on the rig. The rig conditions, the drilled formation, and the drillstring mechanical features influence the transmission modes and the quality of the pilot signal. Other factors that can influence the signal and noise propagation are the borehole conditions and the surrounding formation properties (Lea and Kyllingstad, 1996).

Many kinds of coherent and random noise components are produced at the rig and yard. Part of this noise, such as human activity and the colored noise of pump strikes, is transmitted to the drillstring. Another source of surface noise is the jumping of the traveling block and surface rig equipment (Aarrestad and Kyllingstad, 1993), the shaking of the hoisting wirelines, and nonlinear random noise effects. Rector (1992) points out and analyzes the drillstring noise caused when the bail and the swivel in a rotary system rub together. He proposes using a triaxial accelerometer to separate this noise. Drill-bit signal and rig noise separation using multiple pilots and statistical independence is also discussed by Poletto et al. (2000)

DRILLSTRING WAVES IN THE CORRELATED DOMAIN

A correct interpretation of drillstring vibrations is important in seismic-while-drilling processing. Among other possible options we use deconvolved correlations to interpret the drillstring waves. Let the pilot signal in the frequency domain be expressed as

$$P = a_{ps} P_S W_S + a_{pn} P_N W_N, \tag{1}$$

where W_S and W_N are, without loss of generality, white sources of bit signal and surface rig noise, respectively; a_{ps} and a_{pn} are real constants; and P_S is the response for the bit signal transmitted through the drillstring from the bit source to the surface pilot. If we separate the transfer function in the composition of a pure delay and of an impulse response with zero-delay time, P_{S0}, we have $P_S = P_{S0} \exp(\imath \phi_{ps})$, where ϕ_{ps} is the phase delay from the bit source to the surface pilot. The value P_N represents the reflectivity response from the drillstring and rig at the pilot sensor location. Here we approximate the surface conditions assuming the surface noise is generated, with a delay equal to zero, at the pilot location. Let D be a one-sided deconvolution operator spiking the pilot trace. In the presence of signal only, we have

$$D_S P \gtrapprox a_{ps} \exp(\imath \phi_{ps}) W_S \tag{2}$$

and in the presence of only noise we have

$$D_N P \gtrapprox a_{pn} W_N \tag{3}$$

with $D_N \neq D_S$.

Further, let the colored seismic signal transmitted through the rocks be given by

$$X = [a_{xs} X_S W_S + a_{xn} X_N W_N] G, \tag{4}$$

where a_{xs} and a_{xn} are real constants, X_S represents the downhole signal with the drillstring reflectivity at the bit, and $X_N = X_{N0} \exp(\imath \phi_{xn})$ is the filter for the surface noise transmitted from the source to the bit location with the phase delay ϕ_{xn}. In our approximation we assume $\phi_{xn} \cong \phi_{ps} = \phi_p$. Finally, G is the bit-to-seismic-receiver response.

Crosscorrelating the deconvolved pilot signal $D_S P$ with the seismic trace X and neglecting the noise term ($a_{ps} a_{xs} \gg a_{pn} a_{xn}$), we obtain

$$\begin{aligned} C_{DS} &= D_S^{\gg} P^{\gg} X = a_{ps} a_{xs} |W_S|^2 \exp(\gg \imath \phi_p) X_S G \\ &\cong a_{ps} a_{xs} \exp(\gg \imath \phi_p) X_S G, \end{aligned} \tag{5}$$

where ($\gg$) denotes the complex conjugate, and

$$\begin{aligned} C_{DN} &= D_N^{\gg} P^{\gg} X = a_{pn} a_{xn} |W_N|^2 \exp(\imath \phi_p) X_{N0} G \\ &\cong a_{pn} a_{xn} \exp(\imath \phi_p) X_{N0} G \end{aligned} \tag{6}$$

for the rig noise, neglecting the signal term ($a_{ps} a_{xs} \gg a_{pn} a_{xn}$). In a similar way, we obtain the (one-sided) deconvolved pilot autocorrelations by

$$A_{DS} = D_S^{\gg} P^{\gg} P = a_{ps}^2 |W_S|^2 P_{S0} \cong a_{ps}^2 P_{S0} \tag{7}$$

and

$$A_{DN} = D_N^{\gg} P^{\gg} P = a_{pn}^2 |W_N|^2 P_N \cong a_{pn}^2 P_N \tag{8}$$

for signal ($a_{ps}^2 \gg a_{pn}^2$) and noise only ($a_{ps}^2 \gg a_{pn}^2$), respectively. However, in the case of a mixture of bit signal and surface rig noise with $a_{ps}^2 \gg a_{pn}^2$, deconvolution using operators derived from pilot autocorrelation may be distorted.

In the following example, we interpret the signal multiples assuming that $a_{ps}^2 \gg a_{pn}^2$. Figure 3a shows deconvolved pilot autocorrelations, where the traces correspond to axial pilot signals acquired at increasing string length. The data are obtained by stacking from 90 to 120 correlations of 24-s field records with a sampling rate of 2 ms. A 2-s deconvolution operator is applied to each trace. The data are filtered in the frequency band from 16 to 46 Hz. We observe the first arrival (event A) aligned at $t = 0$ s; interpreted as a bit signal, it corresponds to the direct arrival from the bit to the surface pilot sensor (because of the autocorrelation, the delay disappears). Event B represents the long multiples of the drillstring, reflected from the rig to the BHA and back to the pilot sensor, with the arrival time increasing according to drillstring length. Event B is used to estimate the velocity of the pilot signal. We can observe a variation of the waveform of the long-period multiple at a depth of 1800 m. This effect is related to a significant change in the drillstring, with a lighter BHA before a depth of 1800 m. This example shows how the interpretation of the phases of the reflected events can be critical for pilot velocity analysis.

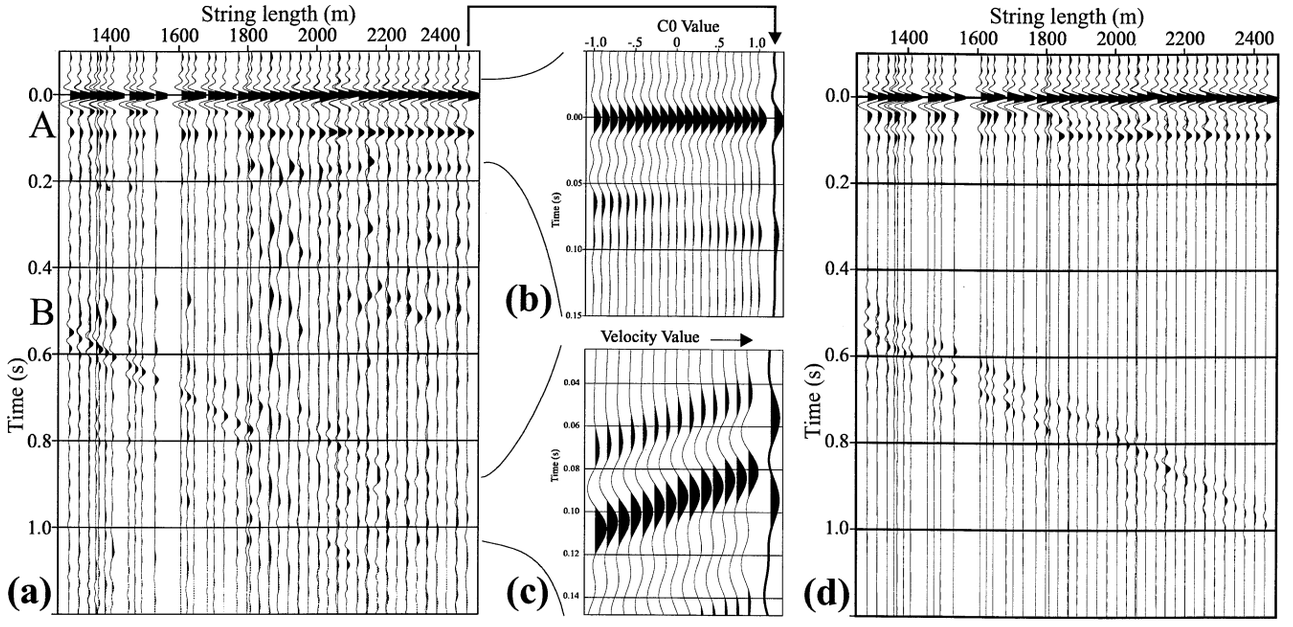

FIG. 3. (a) Example of deconvolved autocorrelations of real pilot data. Event A corresponds to the drill-bit signal first arrival aligned at $t = 0$ s. Event B represents the drillstring long-period multiples of the bit signal acquired at increasing string length. The features of both these events mainly depend on BHA composition and boundary conditions. To determine the optimum $\hat{c}_0$, we compare a series of synthetic traces, obtained by varying c_0, with the corresponding real trace represented on the right side of panel (b). To determine the optimum velocity, we compare a series of synthetic traces, obtained by varying the drill-pipe average velocity, with the corresponding real trace shown on the right side of panel (c). The synthetic surface pilot seismograms with the first arrival aligned at $t = 0$ s (d) best fits the real data. The waveform variation at a depth of 1800 m, also observable in the real data (a), is related to a significant change of BHA composition.

MODELING DRILLSTRING AXIAL AND TORSIONAL WAVES

In acoustics, a transmission line is composed of a tube in which a vibration propagates. Any interface between two tubes with different acoustic impedance is characterized by a reflection coefficient c and a transmission coefficient t. In a sequence of tubes with different acoustic properties, we obtain a cascade of reflections.

In considering the drillstring as a sequence of cylinders with different lengths and weights (see Figure 2) in which the mechanical properties are constant, we model it as a 1-D system of blocks with different acoustic impedances. In our approximation, each section of different type drill pipe is a continuous, homogeneous system with constant mechanical characteristics and diameters. In fact, propagation in the drill pipe generates effects of band-pass filter for axial and torsional waves that are undetectable in the frequency band used in the seismic-while-drilling technique, whose frequencies are <120 Hz.

We close the drillstring transmission line with surface and downhole boundary conditions. At the surface, the top of the drillstring is coupled to the rig structure by means of a reflection coefficient c_T. The rig is described by reflection coefficients and assuming in the simplified condition that an escaping wave E_W is transmitted from the rig to the ground. Downhole, the bit is coupled to the formation by a reflection coefficient c_0. This depends on the variation of the acoustic impedance between bit and rock and on the drilling conditions.

A recursive algorithm describes the propagation of acoustic waves in a transmission line (Claerbout, 1976). Let the propagation in the transmission line be represented by the Z-transform of the time series, defined as $a_0 + a_1 Z^{\gg 1} + \lll\lll + a_j Z^{\gg j} + \lll\lll$ for time series a_j. Let the one-way delay in each discrete element of the transmission line be equal to $Z^{\gg 1/2}$. Let c_j and t_j be the reflection and transmission coefficients, respectively, of the jth interface of the transmission line. It holds that $t_j = 1 + c_j$. The well-known propagation matrix, which allows us to compute the downgoing and upgoing waves at each interface, is given by

$$M_K = \frac{Z^{K/2}}{\prod_{i=1}^{K} t_i} \begin{bmatrix} F_K(Z) & Z^{\gg K} G_K(Z^{\gg 1}) \\ G_K(Z) & Z^{\gg K} F_K(Z^{\gg 1}) \end{bmatrix} \tag{9}$$

where

$$\begin{cases} F_K(Z) = F_{K\gg 1}(Z) + c_K Z^{\gg 1} G_{K\gg 1}(Z) \\ G_K(Z) = c_K F_{K\gg 1}(Z) + Z^{\gg 1} G_{K\gg 1}(Z) \end{cases}. \tag{10}$$

Recursions (10), together with the initial conditions $F_1 = 1$ and $G_1 = c_1$, give the functions $F_K(Z)$ and $G_K(Z)$ from reflection coefficients c_k, with $k = 1, \ldots, K$. This algorithm allows us to calculate the propagating signal in any position of the transmission line, after introducing a codified signal, e.g., an impulse or a colored signature. In the general approach, we use two propagation matrices, M_H^{string} and M_L^{rig}, to describe the propagation in the drillstring and rig systems, respectively. The matching conditions between upgoing and downgoing waves at the pilot sensor location and at the bit for the propagating drill-bit signal and for the propagating surface rig noise are computed in the Appendix (see Figure 4). From these relations we obtain, with $Z = \exp(\imath\omega)$, the surface and downhole synthetic seismograms of $P_S(Z)$, $P_N(Z)$, $X_S(Z)$, and $X_N(Z)$ of equations (1) and (4).

Absorption effects are considered using $Z = \exp(\imath\omega')$ with the complex frequency $\omega' = \omega \gg \imath\phi f \triangle t/Q$, where f is the frequency (in hertz) and $\triangle t$ is the sampling rate (in seconds). For axial waves with a central frequency of 30 Hz, a realistic value of attenuation obtained by analyzing the multiples of the one-side-deconvolved pilot correlations after normalizing the direct arrivals, is 6 dB/km.

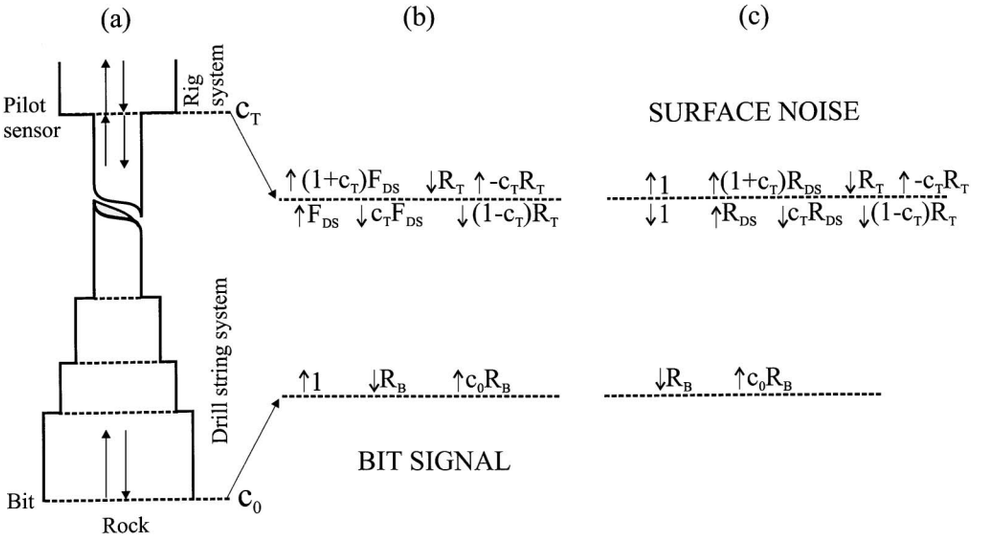

FIG. 4. (a) Boundary conditions for the drillstring and rig transmission lines. The drillstring is coupled to the rock by means of the reflection coefficient c_0 and to the rig system by means of the reflection coefficient c_T. We consider (b) the upgoing and downgoing waves produced by a unit signal and (c) the upgoing and downgoing waves generated by a unit noise pulse at the surface pilot location.

Reflection coefficients in the drillstring

We compute the reflection coefficients for axial and torsional waves in strings formed with tubes of different materials and properties. Let z be the axial coordinate. Assume two string blocks with density, cross-section, Young, and shear moduli $(\phi_1, A_1, E_1, \phi_1)$ and $(\phi_2, A_2, E_2, \phi_2)$, respectively. The matching conditions at the interface are

$$\begin{cases} u_1 = u_2 \\ E_1 A_1 \dfrac{\partial u_1}{\partial z} = E_2 A_2 \dfrac{\partial u_2}{\partial z} \end{cases} \tag{11}$$

and

$$\begin{cases} \phi_1 = \phi_2 \\ \phi_1 I_1 \dfrac{\partial \phi_1}{\partial z} = \phi_2 I_2 \dfrac{\partial \phi_2}{\partial z} \end{cases} \tag{12}$$

for axial and torsional waves, respectively. The symbols u_1, u_2, ϕ_1, and ϕ_2 denote the relative axial and angular displacements, and I_1 and I_2 denote the polar momenta of inertia. For a tube with internal and external radii r_I and r_E, respectively, $I = (\phi/2)(r_E^4 \gg r_I^4)$.

However, for our purposes the string can be considered a rod. When the wavelength of the propagating wave is large with respect to the lateral dimensions of the rod, the theoretical velocities of axial and torsional waves (Kolsky, 1953) are given by

$$V_{ax} = \sqrt{\frac{E}{\phi}} = \sqrt{\frac{EA}{m_{ax}}} \tag{13}$$

and

$$V_{tor} = \sqrt{\frac{\phi}{\phi}} = \sqrt{\frac{\phi I}{m_{tor}}}, \tag{14}$$

respectively, where m_{ax} (kg/m) is the linear density of the mass in the string and m_{tor} (kgm) represents the polar momentum of inertia of the string mass for unit length, respectively, defined by

$$\begin{aligned} m_{ax} &= \phi A \\ \text{and} \qquad & \\ m_{tor} &= \phi I. \end{aligned} \tag{15}$$

Assuming $\phi = 7840$ kg/m^3, $E = 206$ GPa, and $\phi = 78.5$ GPa, the theoretical velocity in a steel rod is $V_{ax} = 5126$ m/s for axial and $V_{tor} = 3164$ m/s for torsional waves.

Inserting a plane wave $\exp[\imath(\omega t \gg kz)]$ with propagation with velocity V and requiring continuity of the frequency $\omega = Vk$ at the interface, from equations (13) and (14) one obtains discontinuity of the wavenumber k with $(k_1/k_2)_{ax} = [(E_2\phi_1)/(E_1\phi_2)]^{1/2}$ and $(k_1/k_2)_{tor} = [(\phi_2\phi_1)/(\phi_1\phi_2)]^{1/2}$ for axial and torsional wavenumbers, respectively. Using these relations and substituting the plane-wave solution in equations (11) and (12), we can see that the reflection coefficient at the interface is

$$c = \frac{a \gg 1}{a + 1}, \tag{16}$$

where a is given by

$$\begin{aligned} a_{ax} &= \frac{A_1}{A_2}\sqrt{\frac{E_1\phi_1}{E_2\phi_2}} \\ a_{tor} &= \frac{I_1}{I_2}\sqrt{\frac{\phi_1\phi_1}{\phi_2\phi_2}} \end{aligned} \tag{17}$$

for axial and torsional waves, respectively. In practical applications, with a simplified approach we assume that the Young and shear moduli of the steel and the density are constant in the string. In this case, the cross-section is proportional to the linear-mass density m_{ax}. In equation (16) we use

$$a_{ax} = \frac{m_{ax,1}}{m_{ax,2}} \tag{18}$$

and

$$a_{tor} = \frac{I_1}{I_2}. \tag{19}$$

In a similar way, we obtain the reflection coefficients for the rig by evaluating the mass distribution of its main blocks, with reflection coefficients close to 1 at the top of the rig and at the kelly bushing interface. A discussion of rig vibration modes is given by Aarrestad and Kyllingstad (1993).

To obtain the position in time of the reflection coefficients used by the recursive algorithms (9) and (10), it is necessary to estimate the axial and torsional propagation velocity. In the initial modeling phase, the distribution of the mass and polar momentum of inertia in reflection time is calculated with the group velocity of axial and torsional waves in a homogeneous steel rod. The group velocity is defined as $V_g = \partial\omega/\partial k$. However, to obtain the group velocity in the drill pipes, we calculate their average elastic properties. In fact, the presence of tool joints which are thicker than the pipe body adds mass to the drill pipes, increasing their stiffness only partially and decreasing the group velocity.

We compute the group velocity from the tables of the drillstring mechanical features using the average values of the linear density of mass and the cross-sections in equations (13) and (14). For axial waves, the average linear mass is obtained by multiplying the steel density by the arithmetic average of the cross-section. Consider, for simplicity, a pipe with density ϕ, body length d_1, and cross-section A_1 coupled with a tool joint of length d_2 and cross-section A_2. We obtain

$$\bar{m}_{ax} = \phi\frac{A_1 d_1 + A_2 d_2}{d_1 + d_2}. \tag{20}$$

On the other hand, the ratio of the force to extension is EA. For a constant force, the stiffness effect is inversely proportional to the cross-section A, and we obtain the average cross-section as

$$\bar{A}_{ax} = \frac{A_1 A_2 (d_1 + d_2)}{A_2 d_1 + A_1 d_2}. \tag{21}$$

Using equations (20) and (21) in equation (13), we obtain the group velocity

$$V_{g,ax} = \sqrt{\frac{E\bar{A}_{ax}}{\bar{m}_{ax}}} = \sqrt{\frac{E}{\phi}}\,\frac{d_1 + d_2}{\sqrt{d_1^2 + \left(\dfrac{A_1}{A_2} + \dfrac{A_2}{A_1}\right) d_1 d_2 + d_2^2}}. \tag{22}$$

Here, we obtain Drummheller's group velocity of axial waves in the low-frequency approximation with a different line of reasoning. For torsional waves we obtain

$$\bar{m}_{tor} = \phi \frac{I_1 d_1 + I_2 d_2}{d_1 + d_2} \tag{23}$$

and

$$\bar{I}_{tor} = \frac{I_1 I_2 (d_1 + d_2)}{I_2 d_1 + I_1 d_2}. \tag{24}$$

Hence, the group velocity is

$$V_{g,tor} = \sqrt{\frac{\phi \bar{I}_{tor}}{\bar{m}_{tor}}} = \sqrt{\frac{\phi}{\phi}} \frac{d_1 + d_2}{\sqrt{\left(d_1^2 + \right)\frac{I_1}{I_2} + \frac{I_2}{I_1}\Big) d_1 d_2 + d_2^2}}. \tag{25}$$

Examples of average values measured in type S drill pipe are $\bar{m}_{ax} = 32.9$ kg/m, $\bar{A}_{ax} = 0.00356$ m^2, $\bar{m}_{tor} = 0.119$ kgm, and $\bar{I}_{tor} = 12 \gg 10^{\gg 6}$ m^4. An example of velocity values computed for drill pipe of different types and for the BHA is shown in Table 2. Since the BHA is more massive than the drill pipe, its group velocity is closer to the theoretical steel-rod velocity.

To obtain the accurate conversion of the axial coordinate in the drillstring reflection time, we use an initial sampling rate of 10 ϕs. Then we resample the distributions of mass and polar momentum of inertia to the sampling rate of the real data (2 ms) and calculate the reflection coefficient time series.

FITTING WITH REAL DATA

Figure 5 shows the computed BHA reflection time series with the mechanical features of the drillstring. Using the reflection coefficients in recursions (9) and (10), we compute the initial synthetic seismogram. To fit the deconvolved autocorrelation of a real pilot trace, we estimate c_0, c_T, and the velocity in the drillstring. Changing the rock-bit coefficient c_0 and the coefficient at the rig c_T in Appendix equations (A-4) and (A-5), we produce a series of synthetic traces. The optimum coefficients $\hat{c}_0$ and $\hat{c}_T$ are obtained with a least-squares minimization of the error between the real and synthetic data in a window centered on the direct drillstring arrival (Figure 3b). This window contains short-period BHA reverberations and rig noise. In this step we also estimate the optimum average propagation velocity in the BHA, $\hat{V}_{BHA}$, and the reflection coefficient at the top of the drillstring, c_T.

Using the optimum $\hat{c}_0$, $\hat{c}_T$, and $\hat{V}_{BHA}$, we produce the synthetic seismograms with different drill-pipe velocities, which are varied within a range of values centered on the theoretical group velocity. Then we estimate the optimum average velocity in the pipe, $\hat{V}_{pipe}$, by the best fitting of the real data in a window centered on the long-period multiples (Figure 3c). Figure 3d

Table 2. Theoretical and measured velocity

Type of pipe	Theoretical V_{ax} (m/s)	Measured $\hat{V}_{ax}$ (m/s)
S	4730	4705 $\gg$ 4745
E	4850	4830 $\gg$ 4860
G	4880	4890
BHA	5100	5050
	Theoretical V_{tor} (m/s)	Measured $\hat{V}_{tor}$ (m/s)
S	2860	2780 $\gg$ 2800
BHA	3140	3100

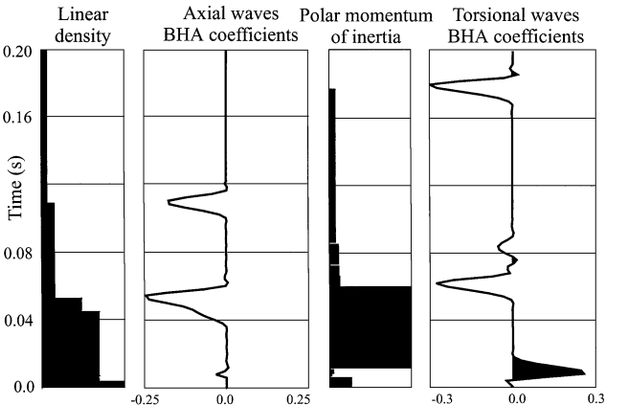

FIG. 5. Using the mechanical description of the BHA and of the different types of drill pipe, we calculate the linear density and polar momentum of inertia and then, assuming as constant the properties of the steel, the reflection coefficient time series in the drillstring for axial and torsional waves. The initial drillstring-length-to-time conversions are obtained using the axial and torsional group velocities in the low-frequency approximation.

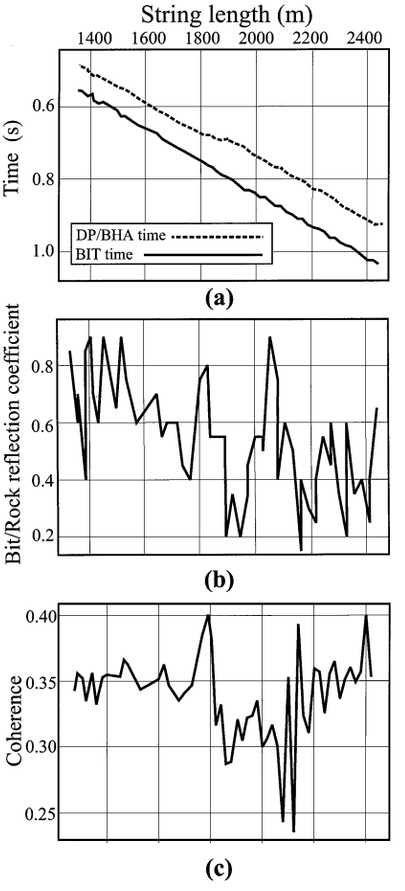

FIG. 6. (a) The bit and drill-pipe/BHA contact points and (b) the bit-rock reflection coefficients c_0 are obtained by least-squares minimization of the difference between real and synthetic data obtained at different bit depths. The coherence of the fitting is displayed for quality control.

shows the synthetic surface pilot seismograms with the first arrival aligned at $t = 0$ s. Figure 6 shows the time positioning of the reflections at the bit and at the contact point between drillpipes and BHA together with the estimated rock-bit reflection coefficients $\hat{c}_0$. The coherence of the fitting is displayed for quality control (Figure 6c).

This procedure (Figure 7) is used in the field to calculate automatically the pilot delay of the bit signal through the drillstring and to convert the correlation time to seismic time for correct positioning of the events measured by the geophones. Because the drillpipe length is much larger than the BHA length, the most critical is the velocity in the drill pipe.

We obtain good agreement between the initial group velocities of axial and torsional components and their measured values $\hat{V}$ for different types of pipe and typical BHAs. For comparison, we also calculated the velocity V_{pick} by picking the times of the long-period multiples of good-quality axial pilot data. We obtained, between V_{pick} and $\hat{V}$, an rms difference of 12 m/s. Typical values of $\hat{V}$ are shown in column 3 of Table 2.

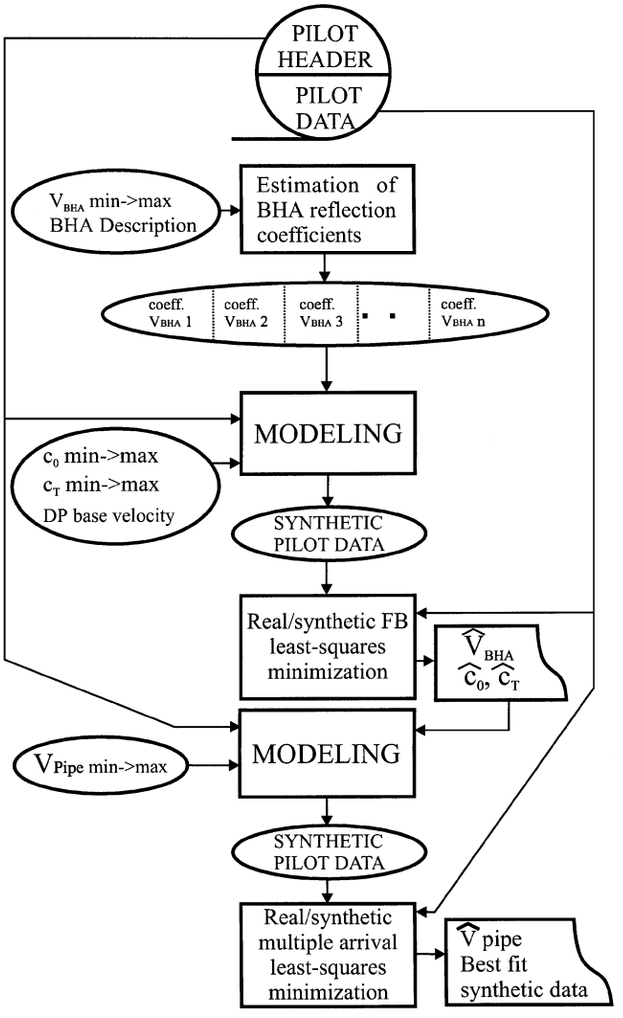

FIG. 7. Layout of the procedure used to automatically calculate the pilot delay of the bit signal through the drillstring. The information used in the trace headers of the real pilot seismograms is used to prepare the synthetic traces to fit with the real pilot data.

The synthetic seismograms in Figure 3d correspond to the real correlations in Figure 3a. Comparing real and synthetic data of this example allows us to interpret the change of the features of the long-period multiple at a depth of 1800 m as the result of a remarkable change in BHA composition. Above 1800 m depth, the reflection at the drill-bit position is observable at its estimated time. Below 1800 m depth, the reflection at the bit is masked by the reflection at the interface between drill pipe and heavyweight pipe.

INTERPRETATION OF DRILLSTRING VIBRATIONS

The following real examples used to interpret drillstring vibrations are obtained mainly using roller-cone data.

Comparison of axial and torsional components

The detection of axial drill-bit multiples can, in some cases, be difficult because of noise and amplitude decay. To get adjunctive information about velocity propagation of elastic waves in the drillstring, we use both axial and torsional components. By crosscorrelating axial and torsional signals from surface pilot components, we measure their relative delay. This is auxiliary information about the drillstring mechanical properties and the propagation velocity of waves. Let $\Delta t_{at} = (t_{tor} \gg t_{ax})$ be the relative time delay between torsional and axial waves. Considering the signals transmitted from the bit through a drillstring with length L_S, we have $t_{ax} = L_S / V_{ax}$ and $t_{tor} = L_S / V_{tor}$. The relative delay gives a relation for the elastic parameters used to describe the drillstring. In fact, from $V_{ax} = (E\bar{A}_{ax}/\bar{m}_{ax})^{1/2}$ and $V_{tor} = (\phi \bar{I}_{tor}/\bar{m}_{tor})^{1/2}$, we obtain

$$\frac{\Delta t_{at}}{L_S} = \sqrt{\frac{\bar{m}_{tor}}{\phi \bar{I}_{tor}}} \gg \sqrt{\frac{\bar{m}_{ax}}{E\bar{A}_{ax}}}. \qquad (26)$$

Equation (26) can be used to verify the pipe-wear state influencing the calculation of the axial and torsional group velocity, depending on the linear mass distribution and the polar momentum of inertia, respectively. For a pipe S with 20% wear, we have a variation of about 2.1% for the axial velocity (4727–4626 m/s) and 2.3% for the torsional velocity (2860–2795 m/s). Figure 8a shows the crosscorrelation of real axial and torsional surface-pilot data. The arrival time of the event, by increasing two-way time according to string length, represents Δt_{at}. Figure 8b shows the crosscorrelation of synthetic axial and torsional surface pilot data, calculated to correctly interpret the delays between torsional and axial signals from among other coherent periodical events in the pilot seismograms. The relative delay of the axial and torsional pilot data is used to calculate the velocity of the pilot torsion waves once the axial velocity is known. These waves can be measured at the surface by pairs of horizontal accelerometers on the top drive or by torsion sensors, such as a current shunt meter applied to the power circuit to measure the motor driving current (Angeleri et al., 1996). Figure 8c is an example of the correlation of the axial and current shunt pilot signals, showing very clear and interpretable torsion delays.

Drillstring multiples in pilot data

In the presence of multiple reflections of the coherent noise, the goodness of the seismic data is not directly related to pilot reverberations. For this reason, we analyze the different contributions of the drill-bit signal and the surface rig noise to

long-period drillstring multiples in the deconvolved pilot autocorrelations. To exploit the arrival times, we simplify the model, considering a single coefficient c_T at the top of the drill pipe. Let t_{0S} be the arbitrary initial time of the signal, and let t_{pipe} and t_{BHA} be the one-way delays in the drill pipe and BHA, respectively. We observe the first long-period multiple of the pilot signal, passing in the BHA three times. Its arrival time corresponds to the event generated at the top of the BHA. In the correlation time, it is given by

$$t_{CPS}^{M1} = t_{0S} + 3t_{pipe} + t_{BHA} \gg (t_{0S} + t_{pipe} + t_{BHA}) = 2t_{pipe}. \quad (27)$$

Figure 9 shows the synthetic and real axial pilot signals.

On the other hand, considering the surface rig noise with an arbitrary initial time t_{0N}, the wavefront propagates downward through the drillstring and rebounds to the surface pilot sensor, passing in the BHA twice. The correlated arrival time of this event is again

$$t_{CPN}^{M1} = t_{0N} + 2t_{pipe} \gg t_{0N} = 2t_{pipe}. \quad (28)$$

Since the correlation times equal in equations (27) and (28), there is some ambiguity in the real data, as they can be caused by both of these events which contribute to the pilot autocorrelation. According to equations (7) and (8), they have a different content of BHA reverberations. This difference can be observed by comparing the synthetic of the drill-bit signal (Figure 9b) with the surface rig noise (Figure 9c). In realistic applications, both signal and noise contribute to the surface pilot deconvolution operator. Surface noise can be produced when the hoisting wirelines and hook shake and jump. Other types of noise sources can be the activity and motion of the top drive on the rail and, at a lower level, rig vibrations transmitted to the rig and pipe (Rector, 1992). The impulse response of the surface pilot is also partially contained in the vibrations radiating from the rig [represented by E_W in equation (A-5)] as surface and direct waves. For this reason, the surface pilot deconvolution operator partially matches the operator for the radiated rig noise. However, equations (5) and (6) and the analysis of the geophone data show that the downhole signal needs a different operator.

Drillstring multiples in geophone data

In many cases, as for roller-cone bit signals acquired when drilling carbonate rocks, periodicities radiated from the bit are very clear and detectable in geophone seismograms (Rector and Hardage, 1992). A case in which the periodicity of the drillstring is particularly evident in geophone data is given by the crosshole geometry. As an example, Figure 10 shows a drill-bit common-source record obtained with three-component (3C) geophones located in a well 500 m from the source well (Aleotti et al., 1999). The vertical components (Figure 10a) show clear S_V arrivals in the formation, with long-period multiples having the periodicity of the drillstring axial waves. In the S_H-oriented components (Figure 10b), the axial periodicity does not appear as clearly.

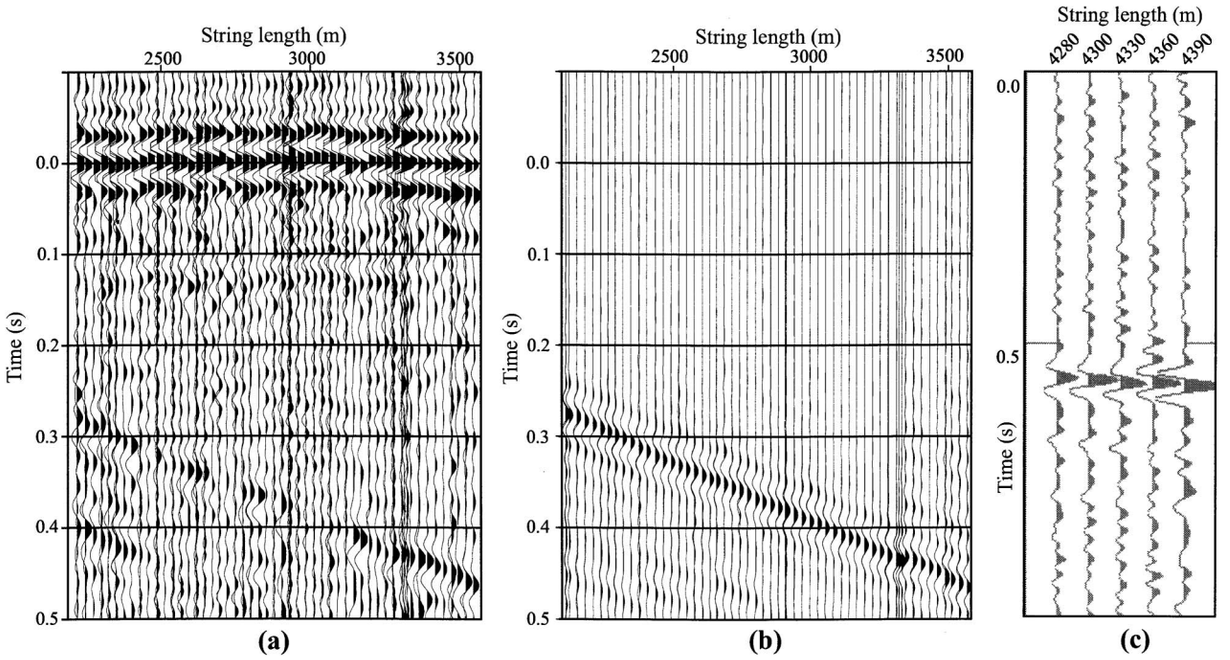

FIG. 8. (a) Real and (b) synthetic crosscorrelation of axial and torsional surface pilot data. The time of the dipping event represents the delay between axial and torsional waves. This auxiliary information about signal propagation in the drillstring can be used to verify the drillstring parameters. The signal can be confirmed by direct torsion measurements. (c) An example of the correlations of the torsion waves measured by a current shunt in another depth interval. These correlations are obtained by using the axial component as the pilot signal.

The schematic in Figure 11a shows the travel path of the bit signal. Part of the wavefront travels through the formations to the surface, where it is recorded by the geophones. Another part travels in the drillstring and is reflected downward from the top of the drillstring. A portion of this wavefront is transmitted into the earth and follows the same path of the direct wavefront. Let t be the bit-to- geophone traveltime through the formation. The first break (FB) arrival time of the direct correlated event is

$$t^D_{CGS} = t_{0S} + t \gg (t_{0S} + t_{pipe} + t_{BHA}) = t \gg t_{pipe} \gg t_{BHA}, \quad (29)$$

while the correlated arrival time of the first multiple is

$$t^{M1}_{CGS} = t_{0S} + 2t_{pipe} + 2t_{BHA} + t \gg (t_{0S} + t_{pipe} + t_{BHA}) = t + t_{pipe} + t_{BHA}. \quad (30)$$

With respect to the FB of the geophone signal [equation (29)], the multiple delay is

$$t^{M1}_{CGS} \gg t^D_{CGS} = 2t_{pipe} + 2t_{BHA}, \quad (31)$$

which is different from the delay of the first long-period multiple in the pilot deconvolved autocorrelation, given by equation (27). This difference appears clearly if we compare the drillstring reverberations of the bit signal in the pilot (Figure 9a) with the geophone data (Figure 12a), which show the reverse VSP correlations of the data recorded by a geophone of the seismic line aligned with $t = 0$ s after FB picking. The event with increasing two-way time according to the string length is the long-period drillstring multiple transmitted in the formation.

However, also for the geophone correlations given by equations (5) and (6), there is some ambiguity in the interpretation of the periodicities since the periodicities of the signal radiated at the bit can be confused with the arrival of the surface rig noise transmitted through the string and then to the formation. In the scheme of Figure 11b, we consider the noise source at the rig. This wavefront propagates in the drillstring, and part of it is transmitted through the bit to the formation and to the surface geophones. The correlation time of the direct arrival is

$$t^D_{CGN} = t_{0N} + t_P + t_{BHA} + t \gg t_{0N} = t + t_{pipe} + t_{BHA}, \quad (32)$$

where we approximate that, because the noise source is placed close to the surface pilot, the pilot delay is in significant. The coherent arrival of the noise has the same time [equation (32)] as the signal multiples [equation (30)]. In fact, for traces with the first break of the signal aligned to 0 s, the noise arrival time is

$$t^D_{CGN} \gg t^D_{CGS} = 2t_{pipe} + 2t_{BHA}. \quad (33)$$

To validate the interpretation, we model both the bit axial signal (Figure 12b) and the rig noise at the geophone aligned with $t = 0$ s (Figure 12c). Here, we do not consider the reflectivity in the rock layers. Because of the complex nonlinear drilling conditions, such as adsorption at the bit, to fit the corresponding synthetic seismogram to the multiple events transmitted into the formation, we consider a trial transmission coefficient at the contact between bit and rock.

RESULT EVALUATION

This analysis shows that the contributions of the signal's multiples and the drillstring noise can be confused in the correlations of the geophone traces or in the aligned FB data. At the same time, with a different interpretation the signal and the noise in the geophone correlations can give information about the pilot delay. In fact, the signal multiple (31) or the correlated noise arrival time [equation (33)] in the geophone seismograms with aligned FB differ, with a relative delay equal to $2t_{BHA}$ from the multiple or noise arrival times in the pilot signal given by equations (27) and (28), respectively. This

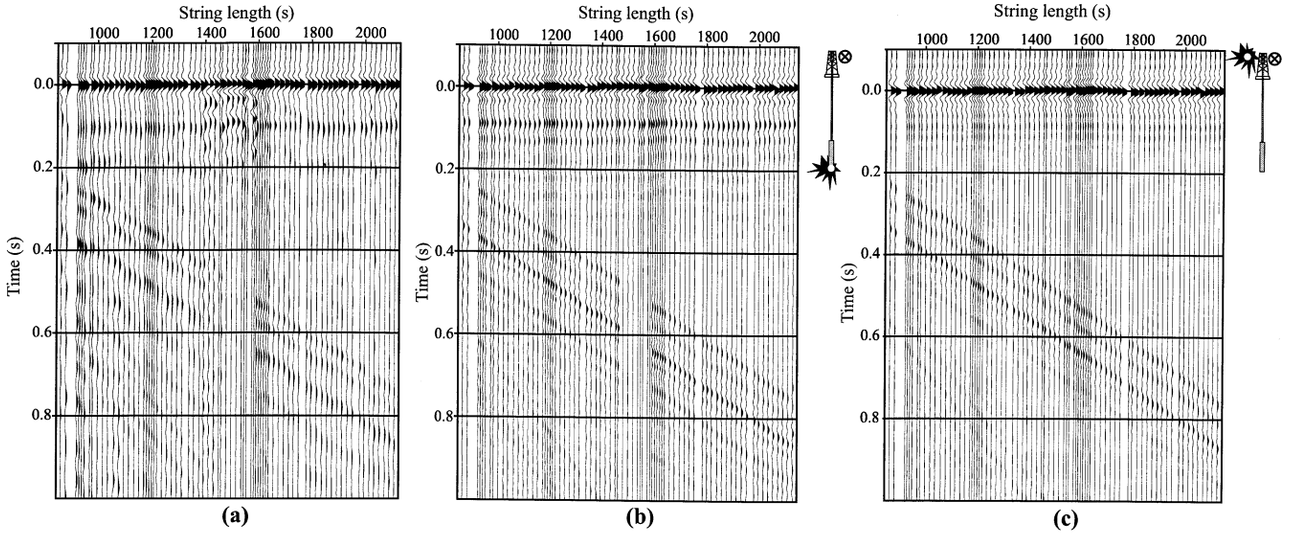

FIG. 9. (a) Example of real surface pilot signal. (b) The corresponding synthetic drill-bit signal. The direct arrival is aligned at 0 s and contains the short-period reverberations of the signal passed once through the BHA. The long-period drillstring multiple contains short-period reverberations of the signal passed three times through the BHA. The direct arrival of the synthetic noise (c) does not contain BHA reverberations, and its long-period multiple contains short-period reverberations of the rig noise passed twice through the BHA.

also makes it clear that pilot surface deconvolution operators are not suited for deconvolving geophone drillstring multiples properly.

We can assume that, in general, the correlated pilot and geophone periodicities contain an ambiguity, since in the real data we can have the different contributions of both the signal and the noise. This may introduce limitations and distortions for drill-bit source deconvolution. Outside of the scope of this work, signal and noise levels could be better evaluated using downhole tools together with surface measurements.

CONCLUSIONS

Our numeric modeling of the rig, drillstring, and rock system is used to characterize the drill-bit source and to interpret the signal transmitted in the formation and in the drillstring. Fitting of the surface seismic drill-bit waves is used for synthesis and interpretation of surface and downhole transfer functions. The main results are the automatic calibration of the propagation velocity of the axial and torsional waves in the drillstring and the verification of the drilling boundary conditions. Again, numeric modeling shows that signal and noise, in corresponding pilot and seismic data, have different but similar trends of periodicity, with the same long-period multiple delay and a different content of short-period BHA reverberations. A similar analysis can help interpret noise components generated at intermediate contact points during deviated drilling. Furthermore, a more effective separation of signal and noise can be obtained with the joint use of downhole and surface measurements.

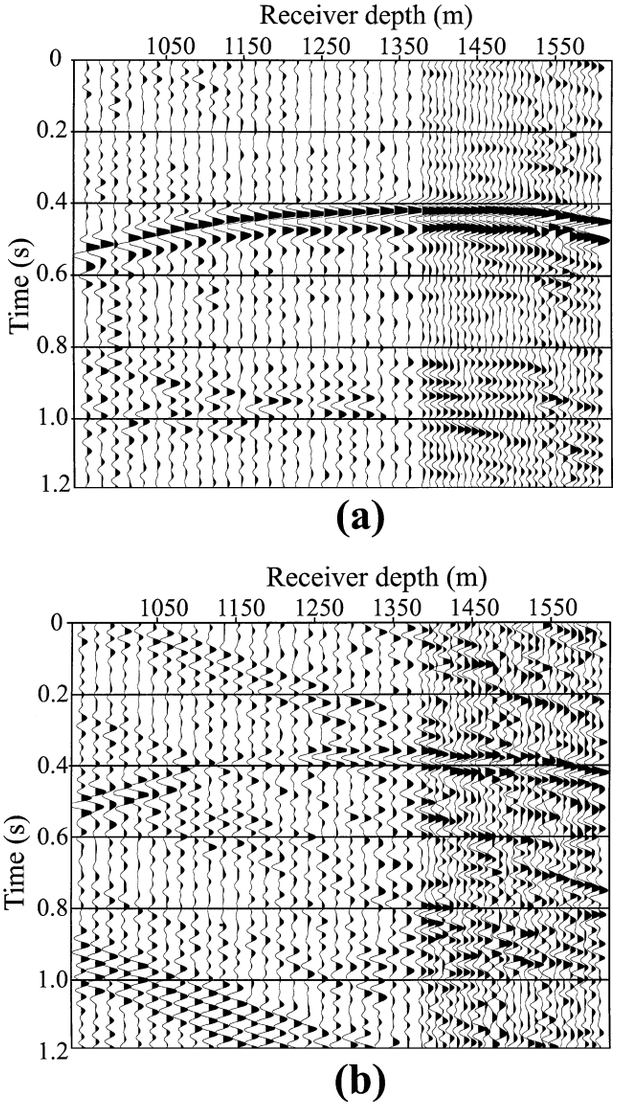

FIG. 10. Example of drillstring periodicity radiated from the bit in a crosshole geometry. The geophone correlations correspond to a common-source gather obtained with a roller-cone bit. The long-period axial drillstring multiples are more clearly detectable in the S_V arrivals (a) than in the S_H arrivals (b).

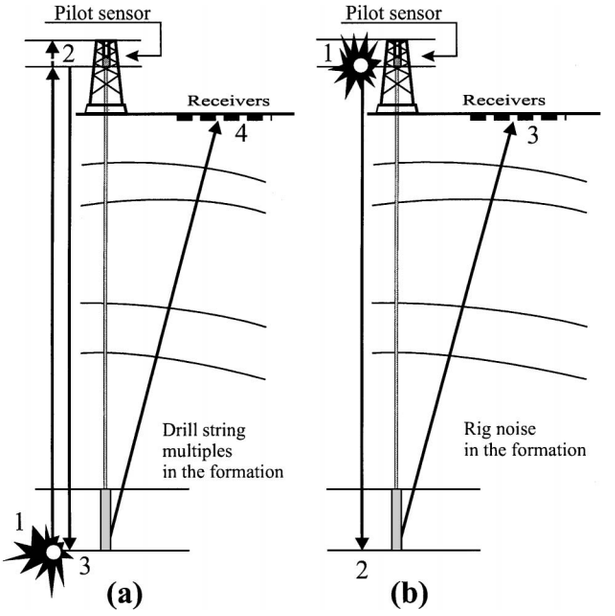

FIG. 11. Scheme of the travel path of (a) the bit signal and (b) the rig noise recorded by the geophones of the surface seismic line.

ACKNOWLEDGMENTS

The authors thank ENI-Agip for permission to publish the data contained in this article. This work has been undertaken with the contribution of the Commission of the UE under the Thermie program, whose decisive support is gratefully acknowledged.

REFERENCES

Aarrestad, T. V., and Kyllingstad, Å., 1993, Rig suspension measurements and theoretical models and the effect on drill string vibrations: Soc. Petr. Eng. Drill. & Compl., September, 201–206, SPE Paper 19553.

Aleotti, L., Poletto, F., Miranda, F., Corubolo, P., Abramo, F., and Craglietto, A., 1999, Seismic while-drilling technology: Use and analysis of the drill-bit seismic source in a cross-hole survey, Geophys. Prosp., **47**, 25–39.

Angeleri, G. P., Persoglia, S., Poletto, F., and Rocca, F., 1996, Process and device for detecting seismic signals in order to obtain vertical seismic profiles during bore drilling operations: U.S. Patent 5 511 038.

Angeleri, G. P., Persoglia, S., Poletto, F., and Valenti, G., 1990, Drill-bit noise as seismic source: New solutions for improved result: 52nd Ann. Internat. Mtg., Eur. Assn. Expl. Geophys., Extended Abstracts, paper B17.

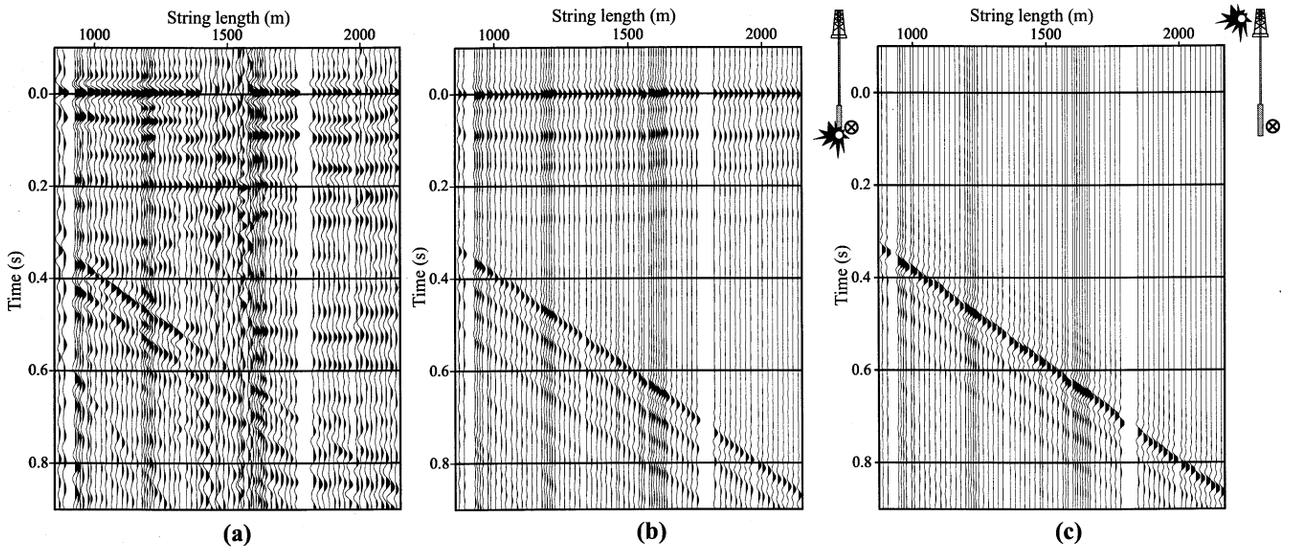

FIG. 12. (a) Example of real reverse VSP correlations of the data recorded by a geophone of the seismic line, aligned at 0 s after FB picking. The events with increasing two-way time according to the drillstring length are the long-period drillstring multiples. (b) The corresponding synthetic traces. The synthetic direct arrival of the rig noise transmitted through the drillstring and bit to the formation (c) is similar to the first long-period multiple of the bit signal.

Barnes, T. G., and Kirkwood, B. R., 1972, Passbands for acoustic transmission in an idealized drill string: J. Acoust. Soc. Am., **51**, 1606–1608.

Booer, A. K., and Meehan, R. J., 1993, Drilling imaging—An interpretation of surface drilling vibrations: Soc. Petr. Eng. Drill. & Compl., 93–98, SPE Paper 23889.

Carcione, J. M., and Poletto, F., 2000, Simulation of stress waves in attenuating drill strings, including piezoelectric sources and sensors: J. Acoust. Soc. Am., **108**, 53–64.

Claerbout, J. F., 1976, Fundamentals of geophysical data processing: McGraw-Hill Book Co., Inc.

Drumheller, D. S, 1989, Acoustic properties of drill strings: J. Acoust. Soc. Am., **85**, 1048–1064.

——— 1992, Extensional stress waves in one-dimensional elastic waveguides: J. Acoust. Soc. Am., **92**, 3389–3402.

——— 1993, Attenuation of sound waves in drill strings: J. Acoust. Soc. Am., **94**, 2387–2396.

Drumheller, D. S., and Knudsen, S. D., 1995, The propagation of sound waves in drill strings: J. Acoust. Soc. Am., **97**, 2116–2125.

Haldorsen, J. B. U., Miller, D. E., and Walsh, J. J., 1995, Walk-away VSP using drill noise as a source: Geophysics, **60**, 978–997.

Hutchinson, M., Dubinsky, V., and Henneuse, H., 1995, An MWD downhole assistant driller: Soc. Petr. Eng., paper 30523.

Kolsky, H., 1953, Stress waves in solids: Oxford Univ. Press.

Lea, L. H., and Kyllingstad, Å., 1996, Propagation of coupled pressure waves in borehole with drillstring: Soc. Petr. Eng. paper 37156, 963–972.

Lutz. J., Raynaud, M., Gastalder, S., Quichaud, C., Raynal, J., and Muckerloy, J. A., 1972, Instantaneous logging based on a dynamic theory of drilling: J. Petr. Tech., 750–758, SPE Paper 3604.

Malusa, M., Poletto, F., Miranda, F., and Bernasconi, G., 1997, SWD interpretation by modelling of pilot and seismic signals: 60th Ann. Internat. Mtg., Eur. Assn. Geosci. Eng., Extended Abstracts, paper 10–51.

Miranda, F., Aleotti, L., Abramo, F., Poletto, F., Craglietto, A., Persoglia, S., and Rocca, F., 1996, Impact of the seismic "while drilling" technique on exploration wells: First Break, **14**, No. 2, 55–68.

Poletto, F., Miranda, F., Corubolo, P., and Abramo, F., 1997, Seismic while drilling using PDC signals—Seisbit experience and perspectives: 59th Ann. Internat. Mtg., Eur. Assn. Geosci. Eng., Extended Abstracts, paper E-053.

Poletto, F., Rocca, F., and Bertelli, L., 2000, Drill-bit signal separation for RVSP using statistical independence: Geophysics, **65**, 1654–1659.

Raynal, J., Barreyre, M., Lutz, J., and Raynaud, M., 1973, Instantaneous logging while drilling: The Aqui-Log/Snap and some possible applications: Soc. Petr. Eng., paper 4489.

Rector, J. W., III, 1989, System for reducing drill string multiples in field signals: U.S. Patent 4 862 423.

——— 1992, Noise characterization and attenuation in drill bit recordings: J. Seis. Expl., **1**, 379–393.

Rector, J. W., III, and Hardage, B. A., 1992, Radiation pattern and seismic waves generated by a working roller-cone drill bit: Geophysics, **57**, 1319–1333.

Rector, J. W., III, and Marion, B. P., 1991, The use of drill-bit energy as a downhole seismic source: Geophysics **56**, 628–634.

Rocca, F., Persoglia, S., Poletto, F., and Craglietto, A., 1990, Use of drilling noise to generate a reciprocal VSP: Final project report, Commission of the European Communities contract DG XVII/TH-0113-87.

APPENDIX

PROPAGATION MATRICES OF SIGNAL AND NOISE

Propagation matrix for a drill-bit signal

Using the notation of Figure 4b, the drill-bit signal in the surface pilot can be written as

$$P_S(Z) = (1 + c_T)F_{DS}(Z) + (1 \gg c_T)R_T(Z). \qquad \text{(A-1)}$$

We represent the propagation matrix (10) computed in the string as

$$M_H^{string} = \frac{Z^{H/2}}{\prod_{i=1}^{H} t_i} \begin{bmatrix} F_H(Z) & Z^{\gg H} G_H(Z^{\gg 1}) \\ G_H(Z) & Z^{\gg H} F_H(Z^{\gg 1}) \end{bmatrix} \qquad \text{(A-2)}$$

and the propagation matrix in the rig as

$$M_L^{rig} = \frac{Z^{L/2}}{\prod_{i=1}^{L} t_i} \begin{bmatrix} F_L(Z) & Z^{\gg L} G_L(Z^{\gg 1}) \\ G_L(Z) & Z^{\gg L} F_L(Z^{\gg 1}) \end{bmatrix}. \quad \text{(A-3)}$$

Inserting a unit bit-signal pulse, the propagation in the drillstring is calculated by

$$\begin{bmatrix} F_{DS}(Z) \\ c_T F_{DS}(Z) + (1 \gg c_T) R_T(Z) \end{bmatrix} = M_H^{string} \begin{bmatrix} 1 + c_0 R_B(Z) \\ R_B(Z) \end{bmatrix} \quad \text{(A-4)}$$

and in the rig by

$$\begin{bmatrix} E_W(Z) \\ 0 \end{bmatrix} = M_L^{rig} \begin{bmatrix} (1 + c_T) F_{DS}(Z) \gg c_T R_T(Z) \\ R_T(Z) \end{bmatrix}. \quad \text{(A-5)}$$

The variables F_H, G_H, F_L, and G_L are the polynomials of the order $H \gg 1$ and $L \gg 1$ describing the propagation in the drillstring and rig, respectively. The variables F_{DS}, R_B, R_T, and E_W are the upgoing signal in the drillstring at the surface pilot location, the downgoing reflected signal at the bit, the downgoing surface signal reflected in the rig system, and the escaping wavefield of the signal radiated from the rig, respectively.

Solving equations (A-4) and (A-5) with respect to $F_{DS}(Z)$, $R_B(Z)$, and $R_T(Z)$, we obtain the surface pilot signal [equation (A-1)] and the downhole signal with the reflectivity at the bit, which is given by

$$X_S(Z) = 1 + (1 + c_0) R_B(Z) \quad \text{(A-6)}$$

for a unit bit signal.

Propagation matrix for rig noise

We approximate the rig noise assuming that the rig noise excitation point at the surface is located in the same position as the pilot sensor. Using the notation of Figure 4c, the rig noise in the surface pilot is given by

$$P_N(Z) = 1 + (1 \gg c_T) R_T(Z) + (1 + c_T) R_{DS}(Z). \quad \text{(A-7)}$$

Inserting a unit rig noise pulse, the propagation in the drillstring is given by

$$\begin{bmatrix} R_{DS}(Z) \\ 1 + (1 \gg c_T) R_T(Z) + c_T R_{DS}(Z) \end{bmatrix} = M_H^{string} \begin{bmatrix} c_0 R_B(Z) \\ R_B(Z) \end{bmatrix} \quad \text{(A-8)}$$

and in the rig by

$$\begin{bmatrix} E_W(Z) \\ 0 \end{bmatrix} = M_L^{rig} \begin{bmatrix} 1 + (1 + c_T) R_{DS}(Z) \gg c_T R_T(Z) \\ R_T(Z) \end{bmatrix}, \quad \text{(A-9)}$$

where, in this case, R_{DS}, R_B, R_T, and E_W are the upgoing reflected noise in the drillstring at the surface pilot location, the downgoing reflected noise at the bit, the downgoing surface noise reflected by the rig system, and the escaping wavefield of the noise radiated from the rig, respectively.

Solving equations (A-8) and (A-9) with respect to $F_{DS}(Z)$, $R_B(Z)$, and $R_T(Z)$, we obtain the surface rig noise [equation (A-7)] and the downhole rig noise transmitted at the bit, given by

$$X_N(Z) = (1 + c_0) R_{TB}(Z). \quad \text{(A-10)}$$